

Hard x-ray continuum crystal spectrograph for inertial confinement fusion (ICF) diagnostics

A. J. Burek, C. J. Armentrout, C. R. Bird, R. E. Frazier, J. B. Geddes, and D. F. Gorzen
KMS Fusion Inc., 700 KMS Place, Ann Arbor, Michigan 48106

(Received 18 April 1991; accepted for publication 3 June 1991)

We describe absolutely calibrated instrumentation for measuring hard x-ray continuum produced during laser irradiation of ICF targets. The instrumentation includes a crystal spectrograph and two collimated filtered scintillators. The absolutely calibrated crystal spectrograph achieves high sensitivity to x-ray continuum over the energy range of 5 to 35 keV with continuous energy coverage and a resolving power $E/\Delta E$ between 20 and 100.

Time integrated spectra are recorded and stored electronically on a shot basis using two dimensional charge coupled device (CCD) camera readout of a proximity focused MCP detector close coupled to the x-ray diffracting crystals. The filtered scintillators provide discrete, time-resolved, high energy channels for recording integrated continuum in the 40–60 and 60–90 keV bands. End-to-end calibration of the crystal spectrograph was performed over the design energy interval. We discuss instrument design, calibration, and alignment and the factors affecting sensitivity and resolving power.

I. INTRODUCTION

Measurement of the high-energy x-ray continuum produced in laser-plasma interactions is an important diagnostic for determining the effect of parametric instabilities on laser-plasma coupling. Understanding these instabilities is an important issue for inertial confinement fusion (ICF) because they produce suprathermal electrons that preheat the ICF target and reduce target compression. The bremsstrahlung continuum produced by suprathermal electrons can extend in energy to hundreds of keV depending on laser driver and irradiance conditions. In the past the primary diagnostic for studying hard x-ray continuum for energies greater than 5 keV has been nondispersive channelized detectors such as filtered scintillators or filtered x-ray diodes.^{1–6} While these detectors have adequate sensitivity they have poorly defined instrument functions that make determination of spectral shape difficult. For the diagnostics planned for Aurora, continuous recording of the hard x-ray spectrum is required over a broad energy range with low to moderate energy resolution. The fact that continuous coverage of the x-ray spectrum is required for a pulsed source suggests the use of dispersive instrumentation using crystals as the dispersive elements.

We describe an absolutely calibrated time integrated crystal spectrograph designed for continuous recording of the high energy x-ray continuum generated in ICF targets. High sensitivity is achieved through efficient crystal geometry and electronic detection. The crystal spectrograph is part of an overall package for high energy continuum diagnostics for the Aurora ICF facility at Los Alamos National Laboratory and also includes two filtered scintillators for time resolved measurements of integrated continuum in the 40–60 and 60–90 keV bands.

II. CRYSTAL SPECTROGRAPH

The design goals for the continuum crystal spectrograph are to provide continuous spectral coverage with

absolute energy and intensity calibration for the energy interval of 5 to 35 keV. Only moderate to low resolving power $E/\Delta E$ of 20 to 100 is required. Sensitivity must be such as to record the continuum expected from hi-Z targets irradiated with kilojoule 0.25 μm laser drivers⁷ while the dynamic range should permit recording the intensity distributions characteristic of 20 to 100 keV continuum temperatures in a single laser shot. In addition, since relatively large laser spot sizes and targets will be used, the required resolving power should be attainable for the maximum anticipated spot sizes with a slitless instrument. Finally, the detector must be compatible with electronic data acquisition and storage and cannot use film.

A. Geometry

Of the many crystal configurations considered only a grazing incidence de Broglie^{8,9} geometry was found to be sufficiently compact that the Aurora target chamber space requirements could be met while still achieving the required energy range for the spectrograph. Laue transmission geometries were also considered and have many advantages^{10–13} in this energy region but could not be used because of the space constraints specific to the Aurora target chamber.

The de Broglie geometry adapted for high energy x rays is shown in Fig. 1. By cylindrically bending a crystal to radius of curvature R through an angular range ψ , a convex curved crystal can diffract a large range of Bragg angles for the small entrance solid angle available in the target chamber diagnostics port. For high energy x rays, Bragg diffraction angles are small and approach grazing incidence for the upper energy range even for crystals having small grating spacing. As a result a large energy range can be diffracted in the forward direction. This results in a diffracted spectrum that is sufficiently compressed that it can be recorded with low energy resolution with a single, compact position sensitive detector. By close coupling the

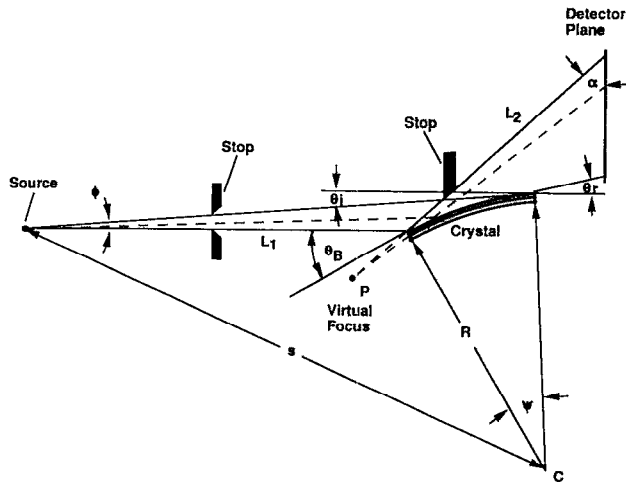


FIG. 1. Geometry for grazing incidence de Broglie Bragg reflection spectrograph.

detector to the crystals it is possible to obtain the low dispersion required for high sensitivity to continuum. Because the crystals have convex curvature, the relative sensitivity compared to a flat crystal is decreased by an amount given approximately by the geometric factor $\phi/\Delta\theta_B$ where ϕ is the angle subtended by the crystal at the source and $\Delta\theta_B$ is the range of diffracted Bragg angles. For the strong curvature required to obtain a large range of Bragg angles, this factor can be quite small. Therefore high efficiency for continuum in this geometry requires large radii of curvature. The main disadvantage of the de Broglie geometry used at grazing incidence is that accurate placement of stops is required to avoid direct beam shine through and prevent background. This makes alignment difficult.

An important feature of the de Broglie geometry is that the convex curvature of the crystal demagnifies the source.^{14,15} If the source width in the plane of dispersion is D , then it can be shown¹⁴ that the projected width at the detector is given by

$$W = \frac{D}{\sin \alpha} \left(\frac{L_2 + r \sin \theta_B}{L_1 + r \sin \theta_B} \right), \quad (1)$$

where L_1 is the distance from the source to the crystal, L_2 is the distance from the crystal to the detector, α is the angle between the detector and the diffracted ray, θ_B is the Bragg angle, and r is the crystal radius of curvature. Since θ_B is small for grazing incidence and L_2/L_1 can be made small by close coupling the detector to the crystal, demagnification is possible. This reduces the effect of source size on energy resolution for a slitless spectrograph.

B. Instrument configuration

A schematic illustration of the 5 to 35 keV continuum spectrograph identifying the major components is shown in Fig. 2 while Fig. 3 shows the detector and collimator assemblies. The crystal spectrograph parameters are given in Table I.

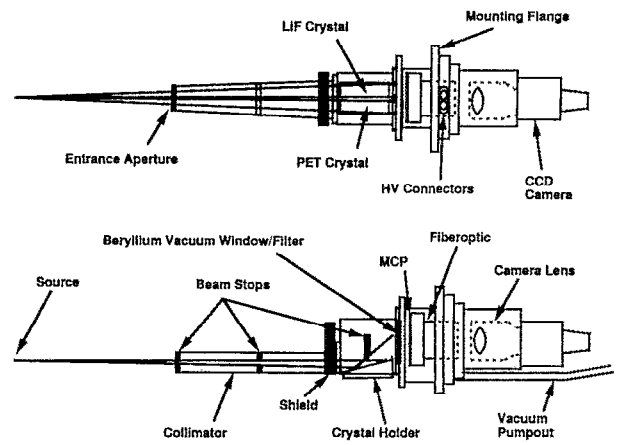


FIG. 2. Schematic diagram of crystal spectrograph showing major components.

The crystal spectrograph utilizes two convex curved crystals mounted side by side on adjustable holders that Bragg diffract incident x rays onto a two dimensional position sensitive detector. The detector is close coupled to the diffracting crystals with the detector plane nearly perpendicular to the line joining the crystal and the source. The spectrograph field of view is defined by a collimator that determines the optical axis to which the crystals are aligned. Crystal mounts and other internal components are made of aluminum to minimize fluorescence. Thick shields mounted externally shadow the sensitive area of the detector from hard radiation while the aluminum housing blocks target chamber fluorescence. A 0.025-cm-thick Be entrance window on the detector vacuum housing provides both a 4 keV low energy cutoff to block internal fluorescence and vacuum isolation for the MCP detector. The detector housing is isolated from the target chamber vacuum and pumped separately to a pressure of less than 10^{-5} Torr. Stop placement, crystal positioning, and adjustment of the dispersion curve for desired characteristics were optimized through ray tracing as part of the CAD mechanical design of the instrument package.

The position sensitive detector consists of a microchannel plate (MCP) proximity focused onto a phosphor coated fiber-optic that relays the image plane of the diffracted spectra to the lens of a charge coupled device (CCD) camera. The spectra can be displayed live on a video monitor or captured and stored on a computer for later analysis.

The LiF 200 ($2d=4.03 \text{ \AA}$) and PET 002 ($2d=8.75 \text{ \AA}$) crystals are both bent to the same radius of curvature of 20.32 cm. The LiF crystal is 4.5 cm long and 1.0 cm wide while the PET crystal is 5.0 cm long and 1.0 cm wide. Both diffract over the same Bragg angle range of 5° to 17° . The grating constants of the crystals are such that there is overlap in the energy range diffracted by each crystal.

The high energy channels consist of two filtered scintillators coupled to fast photomultiplier tubes for wide band time resolved measurements of continuum at energies of 40–60 and 60–90 keV. The energy band of interest is

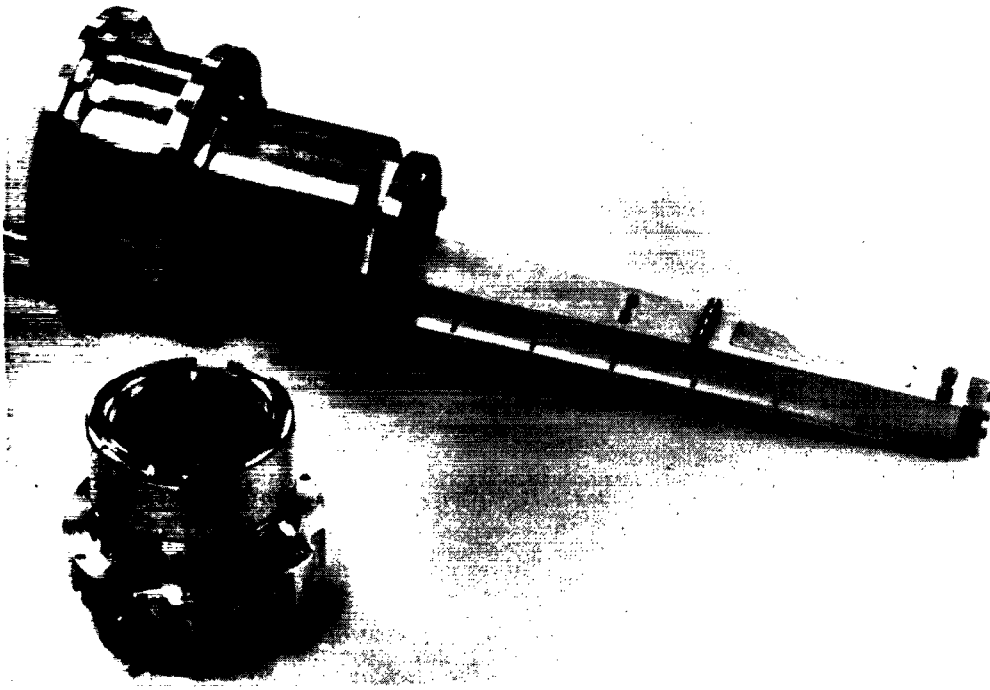


FIG. 3. Crystal spectrograph housing, collimator, and MCP detector.

defined by *K*-edge filters while scintillator material and thickness determines the upper energy limit for response to continuum. Cesium fluoride 2 mm thick is the scintillator material for both channels. The filters are 1.0-mm-thick lead for the 60–90 keV channel and 0.5-mm-thick tantalum for the 40–60 keV channel. The field of view around the source is defined by adjustable collimators.

Cesium fluoride was chosen for the scintillator material to obtain the required time resolution of 2 to 5 ns. Cesium fluoride has good x-ray absorption efficiency for this energy region, can provide a reasonably sharp high energy cutoff and has the shortest decay time for the inorganic scintillators. The scintillation efficiency is about 5% that of NaI and the decay time is about 5 ns. The scintillator is coupled to a 19 mm Hamamatsu R1450 photomultiplier tube (PMT) that has good timing characteristics and low noise. Pulse height spectra show a well-defined photopeak for 45 keV x rays that is cleanly separated from electronic noise. Data from the high energy channels are sent to transient digitizers for time resolved information, and to CAMAC compatible charge integrators for intensity information.

The entire instrument package is illustrated in Fig. 4. A re-entrant design is used with all instruments mounted

in a common housing. The camera, PMTs, and associated electronics are located in air and are electrically isolated from target chamber ground. Beryllium windows in the crystal spectrograph detector housing and high energy channel collimators provide the vacuum interface. The package fits inside a six inch diameter tube and is mounted with a standard eight inch conflat flange to a six inch port on the Aurora target chamber.

C. Continuum sensitivity

For continuum the number of diffracted photons per unit area in the detector plane is given by

$$\frac{dN}{dA} = \sin \alpha \frac{N_s}{4\pi r L} \frac{E}{\tan \theta_B} GDR_c \quad (2)$$

where¹⁶

TABLE I. Crystal spectrograph parameters.

Crystals: PET 002, $2d = 8.75 \text{ \AA}$
LiF 200, $2d = 4.03 \text{ \AA}$
Radius: 20.32 cm
Bragg angle: $5^\circ - 17^\circ$
Crystal width: 1.0 cm
Crystal length: 5.0 cm (PET)
4.5 cm (LiF)
Source to crystal distance: 37.5 cm
Detector to crystal distance: 1.8 cm

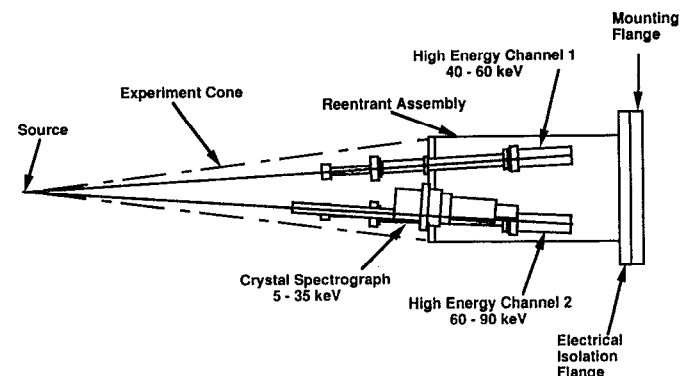


FIG. 4. Schematic diagram of overall instrument package showing re-entrant assembly.

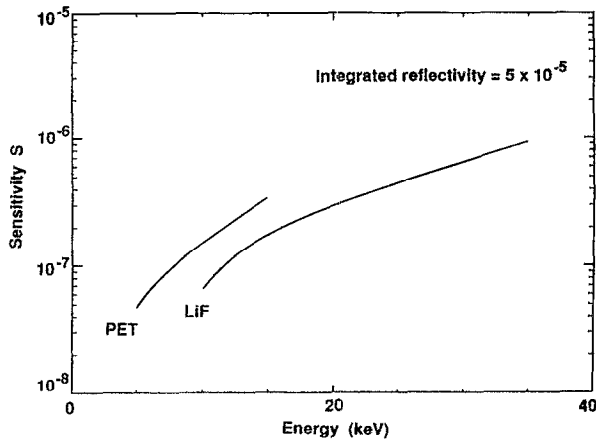


FIG. 5. Sensitivity function calculated for de Broglie crystal spectrograph.

$$G = \frac{d\theta_i}{d\theta_B} = \left(1 + \frac{s^2 - R^2}{R^2 \sin^2 \theta_B} \right)^{1/2} \quad (3)$$

and

$$D = \frac{d\theta_B}{d\theta_r} \quad (4)$$

Here N_s is the number of photons/keV emitted into 4π steradians by the source, α is the angle the diffracted ray makes with the detector, E is the x-ray energy in keV, L is the total x-ray pathlength, r is the distance from the virtual focal point to the detector, θ_B is the Bragg angle, θ_i and θ_r are the relative angles of incidence and reflection, R is the radius of curvature of the crystal, and s is the distance from the source to the crystal center of curvature. In terms of this equation it is possible to define a sensitivity S that characterizes the response of a particular crystal geometry to continuum:

$$\frac{dN}{dA} = SN_s \quad (5)$$

The quantity S is shown in Fig. 5 calculated for a de Broglie geometry with the present configuration. The calculation is for an integrated reflectivity of 5×10^{-5} and assumes that the integrated reflectivity does not change with energy. The curves are for two crystals having the same radius of curvature, intercepting identical Bragg angles but with different grating spacings. It is seen that the sensitivity increases with energy. This is due to the low dispersion at high energy in the present geometry. This has the effect of decreasing the dynamic range requirements of the detector for coronal continuum where the intensity typically falls off exponentially with energy.

D. Resolving power

The crystal spectrograph was designed with a dispersion at the MCP detector such that a detector resolution element of $500 \mu\text{m}$ corresponds to a minimum resolving

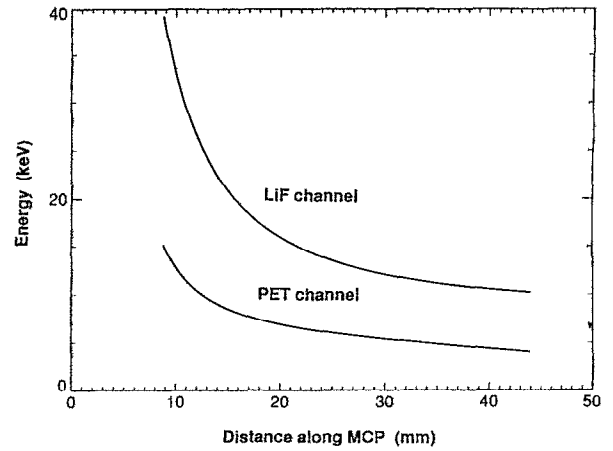


FIG. 6. Dispersion curves giving energy vs position along detector for geometry adopted for crystal spectrograph.

power of about 20. Dispersion and theoretical resolving power for a detector pixel of $500 \mu\text{m}$ are shown in Figs. 6 and 7.

A $500 \mu\text{m}$ detector resolution element was chosen based on conservative estimates of the individual factors that contribute to the overall resolution. These are geometrical broadening due to finite source size, crystal rocking curve, MCP spatial resolution, CCD camera resolution, camera lens quality, and frame grabber digitization resolution. Each of these distributions may be assumed to combine in quadrature when projected onto the fiber-optic image plane.

For a slitless instrument the effect of finite source size is to decrease resolving power by an amount dependent on the size of the source projected onto the detector plane. In the present case this is reduced by the convex curvature of the crystals which has the effect of demagnifying the projected size of the source by an amount given by Eq. (1). For this instrument the demagnification varies between 0.25 to 0.17.

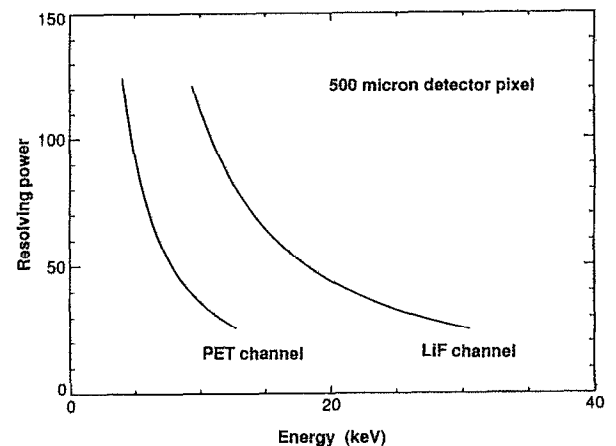


FIG. 7. Theoretical resolving power of crystal spectrograph calculated for $500 \mu\text{m}$ detector resolution element.

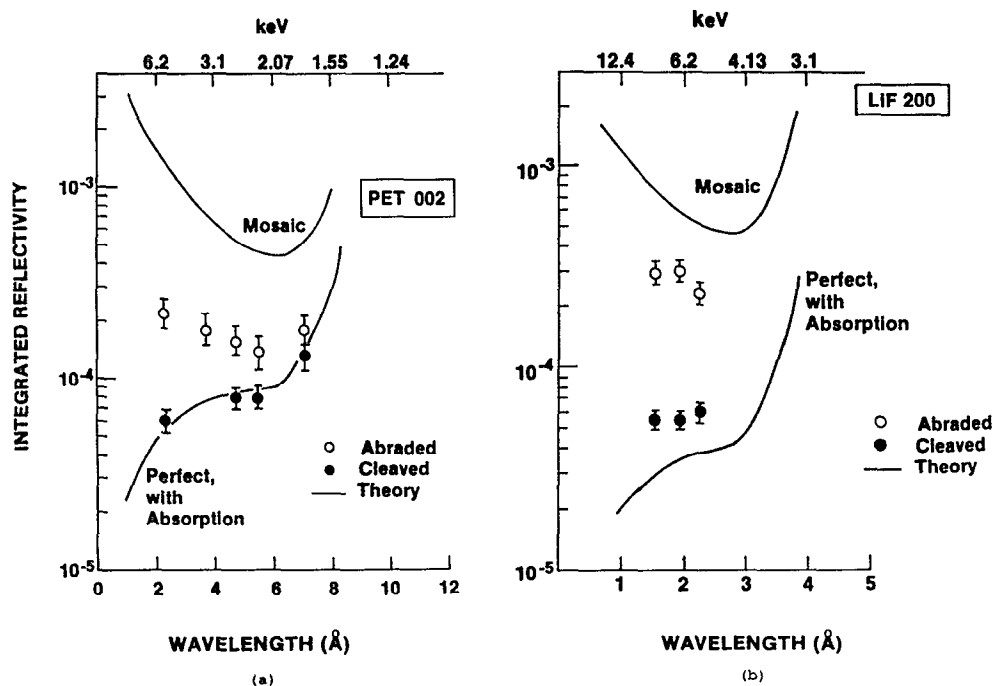


FIG. 8. Measured vs calculated integrated reflectivity for (a) PET 002 and (b) LiF 200 (from Ref. 12).

The rocking curve contribution to the resolving power depends on the quality and preparation of the crystals. The crystals employed were made highly mosaic to increase the integrated reflectivity leading to expected rocking curve widths due to mosaic spread of the order of 1–3 arcmin.¹² This results in a 100 to 350 μm blur when projected onto the MCP. However, for diffraction from mosaic crystals, mosaic focusing reduces the blurring from that expected from mosaic spread.^{11,17} Although the conditions for this design do not maximize this effect some improvement in the resolution due to mosaic focusing is expected.

The spatial resolution of the proximity focused MCP is determined primarily by the lateral diffusion of the electron cloud in transit between the rear surface of the MCP and the phosphor. This is a function of the MCP operating voltages, x-ray energy, and x-ray incident angle. In particular, for the high energy x rays used for this instrument, the radiation is penetrating and the spatial resolution is expected to be degraded, especially at large angles of incidence where several adjacent channels might be activated from a single photon event. Measurements with similar proximity focused MCP detectors with low energy x rays show a typical spatial resolution of the order of 40 μm for 40% MTF for the voltages used here for normal incidence x rays.¹⁸ With the lens magnification required to image the fiber optic onto the CCD the frame grabbed image element size projected onto the fiber-optic image plane becomes about 90 μm . This is larger than the expected MCP resolution. It is also larger than the projected CCD pixel size since the frame grabber spatial digitizing frequency is smaller than the CCD pixel spatial frequency.

III. CRYSTAL SELECTION AND PREPARATION

PET 002 and LiF 200 are used as the diffracting crystals because of their high reflectivity and the fact that they

have low-Z atomic constituents that minimize fluorescence. Neither has an absorption edge in the large energy range that must be covered that would complicate continuum analysis from anomalous dispersion effects. Their grating constants are such that the required energy range can be covered with sufficient overlap for cross calibration.

A comparison of theoretical and measured integrated reflectivity for these crystals is shown in Fig. 8.¹² It is a property of both crystals that they can be made highly mosaic to increase integrated reflectivity. This is important at grazing incidence because the theoretical mosaic integrated reflectivity for ideally mosaic crystals increases strongly at small Bragg angles due to decreasing absorption and lack of primary extinction. By contrast, the integrated reflectivity for perfect crystals goes to zero at small Bragg angles. For real mosaic crystals primary extinction is never completely eliminated and the theoretical curves provide only upper limits to the integrated reflectivity. Both LiF and PET have low intrinsic absorption and the mosaic integrated reflectivity for these crystals can exceed 10^{-4} for the energy range of interest. The rocking curves produced by inducing mosaic structure in LiF or PET will be symmetric and uniform if the initial crystal is free from defects.¹²

PET crystals for use in the spectrograph were prepared by cleaving $10 \times 50 \times 0.25$ mm plates from a $10 \times 50 \times 5$ mm blank. Integrated reflectivity measurements made on freshly cleaved plates at $\text{CuK}\alpha$ (8.05 keV) were close to theoretical indicating nearly perfect crystals. The cleaved plates were bent and attached to convex curved aluminum substrates with UV curing optical epoxy, then abraded with 400 grade SiC abrasive to increase the integrated reflectivity. Similar surface treatment with flat crystals from the same blank gave integrated reflectivities at $\text{CuK}\alpha$ exceeding 10^{-4} .

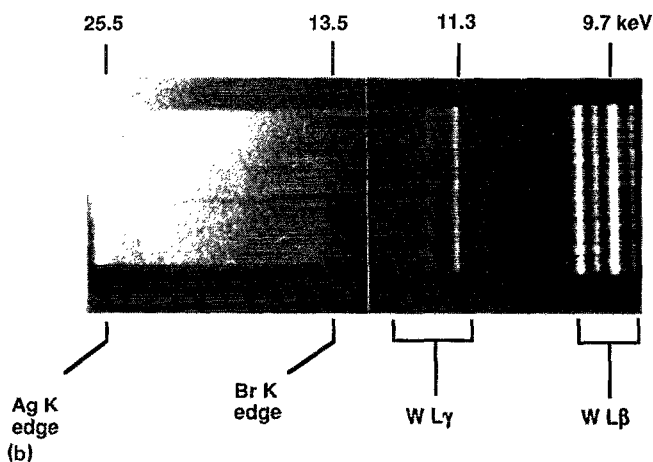
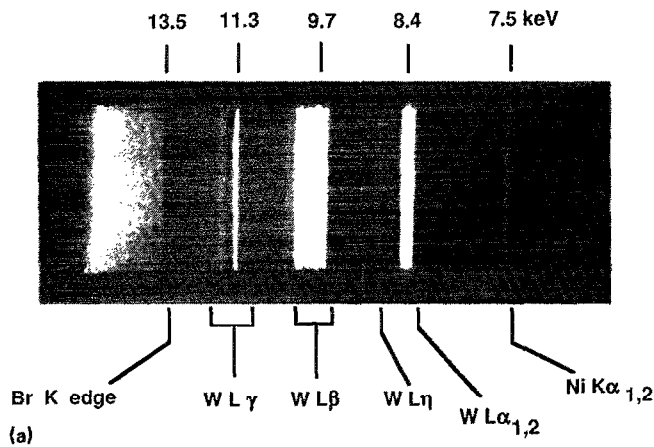


FIG. 9. (a) Spectrum recorded on film of tungsten source with curved, mosaic PET 002 used in spectrograph. Lines are tungsten *L*-series. Continuum break is the bromine *K*-edge in the film emulsion at 13.5 keV. Energy range is approximately 5.5 to 15 keV. Resolving power is about 350 at the center of the spectrum. (b) Spectrum recorded with same conditions with curved, mosaic LiF 200. Continuum break at far left is silver *K*-edge in film emulsion at 25.5 keV. The bromine *K*-edge is near the center of the spectrum. The energy range is approximately 9.5 to 30 keV. Resolving power is about 1500.

Cleaved LiF plates were evaluated for uniformity prior to bending using Berg topography at grazing incidence with continuum produced by a tungsten anode operated at 40 kV. Screening with x rays is necessary for LiF because these crystals can have large scale inhomogeneities that result in nonuniform integrated reflectivity. Those plates that showed adequate x-ray uniformity were abraded with 320 grade SiC to increase the integrated reflectivity. Bending to a radius of 20.32 cm was done plastically at a temperature of 350 °C with a press that compressed the crystal between a convex mandrel and a concave block. Plates with thickness ranging from 0.5 to 1.0 mm were bent this way. Heat soaking the curved crystal for several hours at 350 °C in a closed press avoids relaxation of the crystal to a radius larger than that of the mandrel. For moderate radii of curvature and high quality crystals this procedure produced crystals with accurate radii of curvature and uniform integrated reflectivity. Upon removal from the press the crystal was attached to the curved aluminum substrate using UV curing optical epoxy.

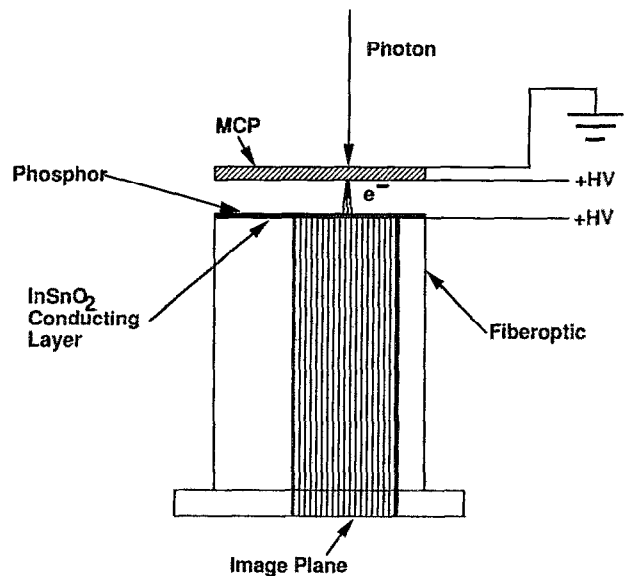


FIG. 10. Schematic representation of proximity focused MCP used in crystal spectrograph.

To determine the quality of the bending and set limits to the crystal resolving power spectra were taken with the curved crystals using film as the detector. Figure 9(a) shows a spectrum recorded on Kodak DEF x-ray film with PET. The geometry is essentially the same as for the spectrograph. The source consists of a slit 250 μm wide backlit by an extended tungsten anode operated at 40 kV. The lines are those of the tungsten *L*-series. It can be seen that the crystal is free from artifacts and that the resolving power is of the order of 350. Figure 9(b) shows a similar spectrum for the highly mosaic LiF 200 crystal after it had been plastically bent and mounted on the curved crystal holder. The geometry is the same as for the PET spectrum. This crystal is also free from artifacts and the resolving power is of the order of 1500. Both crystals show excellent uniformity to continuum.

IV. DETECTOR

The MCP detector for the spectrograph is a modified model XUV-2000 BrightViewTM image converter from KMS Fusion Inc. It uses a nichrome coated 40:1 MCP proximity focused to a phosphor-coated fiber-optic (Fig. 10). MCP pore diameter is 10 μm with 12 μm pore separation. The fiber-optic is untapered with a clear aperture of 40 mm and numerical aperture (N/A) = 1. The phosphor used is P-20 for efficient coupling to the camera CCD. Phosphor thickness is of the order of 3–5 $\mu\text{g}/\text{cm}^2$ and is as thin as possible to enhance image brightness. The phosphor is deposited on a layer of InSnO₂ (conductivity of approximately 50 Ω/square) sputtered onto the fiber-optic to provide an electrical ground return. The MCP to phosphor distance is 750 μm . Because of its stability and adequate sensitivity at high x-ray energies^{19,20} bare nichrome was used as the MCP photocathode. The design is such that different coatings and geometries are possible to accomo-

TABLE II. Detector parameters.

Type: Proximity focused MCP
Aperture: 40 mm diameter
Filter: 10 mils beryllium
MCP: Galileo MCP-40/12, 10 μm channels on 12 μm centers, 40:1 aspect ratio
Coating: Nichrome
Phosphor: P-20
Phosphor thickness: 3–5 $\mu\text{g}/\text{cm}^2$
Fiber-optic conductive coating: InSnO ₂ , 50 Ω/square
Phosphor/MCP spacing: 750 μm
Fiber-optic: 10 μm , N/A = 1, 1.72 in. active diam, untapered
Camera: Cohu 6500 CCD (RS-170, 30 frames/s, field interlace, frame transfer)
Camera/fiber-optic coupling: Cosmicar 8.5 mm, f/1.5 lens magnification = 0.137
Pickup area: 6.4 mm \times 4.8 mm ($\frac{1}{2}$ in. format)
Active elements: 739 \times 484
Cell size: 8.5 μm (H) \times 19.75 μm (V)
Frame grabber: PC Vision Plus
ADC resolution: 8 bits
Image area: 512 \times 512 pixels

date different experimental requirements. Detector parameters are summarized in Table II.

The MCP housing is isolated from the target chamber vacuum and is pumped continuously by an 8 ℓ/s vacuum pump at a pressure at or less than 10^{-5} Torr. The pressure is sufficiently low to allow high gain MCP operation without ion backstreaming. Electrical connections to the MCP are made through the vacuum housing using subminiature high voltage connectors rated for 12 kV.²¹ The detector is operated with the MCP front surface and phosphor at high voltage. Provision is made for alternate grounding arrangements if necessary. With this biasing configuration instrument ground can be easily isolated from the target chamber ground.

The fiber-optic is lens coupled to the CCD camera. The camera is a Cohu 6500 and uses the TC-243 CCD chip. Pixel size is nominally 8.5 μm (H) \times 19.8 μm (V) with an array size of 739 \times 484 active pixels and 8 mm diagonal. Actual pixel size for a given field is 8.5 μm square since half of the well is used for alternate fields. The TC-243 CCD uses a frame transfer architecture (RS-170, 30 frames/second with field interlace) and incorporates on chip correlated double sampling. This provides an order of magnitude reduction in readout noise over comparable CCD cameras and greatly improves camera sensitivity. Integration periods as long as ten frames are possible at room temperature before dark noise becomes objectionable. Although fiber-optic coupling is more efficient than lens coupling the camera has sufficient sensitivity using a f/1.5, $f=8.5$ mm Cosmicar lens to record single photon events when the MCP is operated at high gain. This sensitivity is considered adequate for this application. Using lens instead of fiber-optic coupling greatly simplifies design and assembly. The remote camera head is sufficiently compact that it can be mounted directly on the spectrograph.

The CCD image field is digitized with an eight-bit

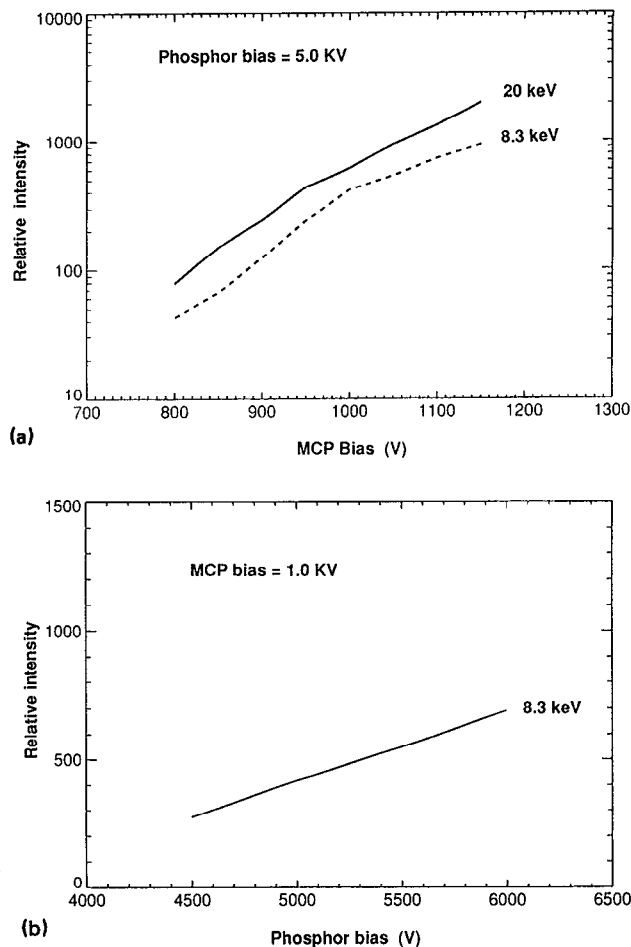


FIG. 11. (a) Characteristic curves showing detector response vs MCP bias for 8.3 and 20 keV x rays. Curves are relative. (b) Relative detector response vs phosphor bias for 8.3 keV x rays.

frame grabber (PC Vision Plus) into a 512 \times 512 array. The magnification of the camera lens required to fill the CCD active area with the fiber-optic display is about 0.14. With this magnification the frame grabber pixel size is larger than the expected MCP spatial resolution. The dynamic range for a specific gain setting of the MCP is determined by the eight-bit resolution of the frame grabber. While this is adequate, improvements are possible by employing frame grabbers with larger ADC resolution. The overall system dynamic range is very large because of the large gain range of the MCP.

The data acquisition system for the crystal spectrograph consists of the frame grabber interfaced to an AT-compatible computer with appropriate control software (VIA-300/286 video image acquisition system from KMS Fusion Inc). In response to an external trigger the camera integrates for two frames then transfers data to computer memory for storage and live image display. The two frame integration period insures event capture but is short enough to avoid dark noise buildup. A blank frame pair is also captured and stored for background subtraction. In the integration mode required for software triggering only a single field is acquired. The microcomputer is networked to a local VAX for data analysis.

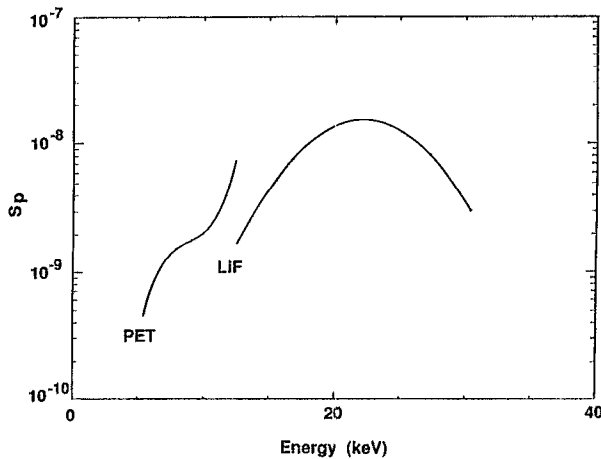


FIG. 12. Measured overall sensitivity S_p for crystal spectrometer. MCP bias = 1 kV, phosphor bias = 5 kV.

Characteristic curves for the detector system are shown in Fig. 11. These give phosphor light output measured by the CCD camera as a function of MCP and phosphor voltages for 8.3 and 20 keV x rays Bragg diffracted by the spectrograph crystals. The incident angles of the radiation onto the MCP are determined by the angle for Bragg reflection from the curved crystals so that these curves are specific to this geometry. The vertical scales are arbitrary and do not indicate the relative sensitivity for the two energies. No evidence was found for changes in detector sensitivity at these energies for total accumulated exposure to x rays of more than several hours.

V. EFFICIENCY CALIBRATION

End to end calibration of the spectrograph was done with continuum x rays generated by a 2.5 kW, 60 kV, sealed x-ray tube with tungsten anode having 500 μm spot size. The tungsten anode at the design target distance provided both strong continuum for intensity calibration and

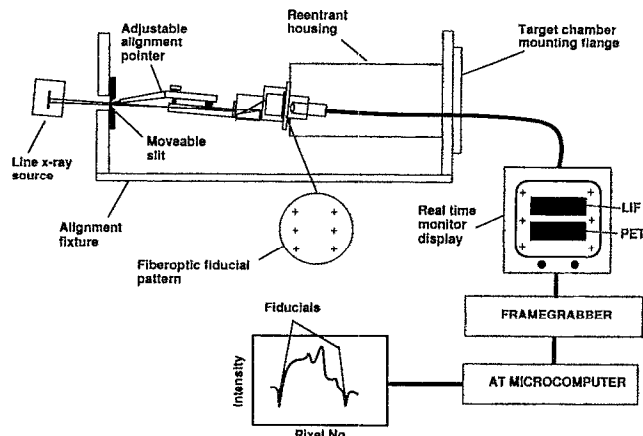


FIG. 13. Bench alignment with x rays for energy scale determination.

strong L -series lines for energy calibration. The instrument was mounted in a test chamber with the x-ray beam path evacuated to less than 10^{-5} Torr. Since the spectrum is predominantly bremsstrahlung continuous sensitivity curves could be derived by relating the digitized spectra obtained with the CCD camera to the incident x-ray flux.

For this application crystal spectrograph sensitivity is given in units that are determined by the digitized CCD camera output for standard settings of the MCP voltages and camera gain. If the camera response for a given x-ray exposure is called R_p and if the incident continuum x-ray flux integrated over an exposure is given as ϕ_v photons/(keV sr), then the sensitivity S_p of the crystal spectrograph is defined so that:

$$R_p = \phi_v S_p \quad (6)$$

where R_p is averaged along the vertical length of the spectrum after subtracting background. The quantity R_p is the value of the eight-bit frame grabber word representing the CCD pixel signal and is a dimensionless quantity ranging from 0 to 255. This can be related to photometric units through separate absolute calibration of the crystals, MCP and CCD camera. However, this is not necessary for an operational determination of overall system sensitivity. The quantity S_p contains the individual instrumental efficiencies and is more accurately measured.

For the efficiency calibration the incident continuum spectrum ϕ_v recorded by the spectrograph was measured directly with a calibrated Si(Li) detector. The spectrograph dispersion curves were used to make the normalizing transformation from the nonlinear spectrograph energy scale to the linear energy scale of the Si(Li) detector. By comparing the continuum data for equivalent energy bins for both spectra the quantity S_p was derived. The MCP characteristic curves are used to relate this calibration to other MCP operating voltages.

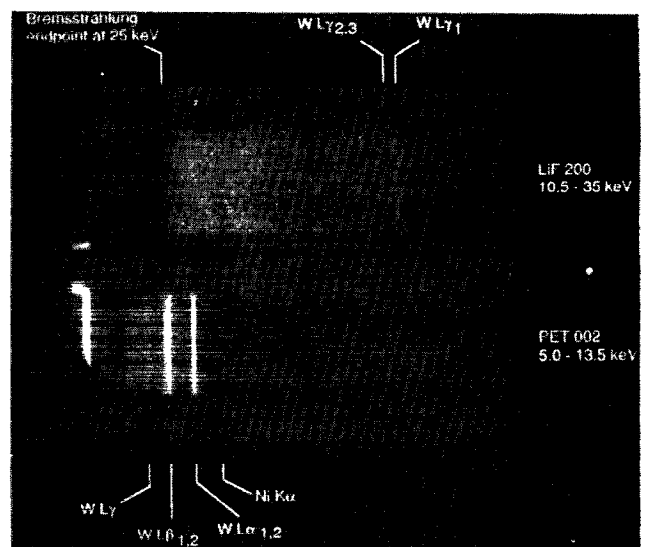


FIG. 14. Live monitor display showing crystal spectrograph output for tungsten continuum source. Source size is 500 μm . Source operated at 25 kV.

The quantity S_p for first-order diffraction from the crystals is shown in Fig. 12. Second order from the PET crystal at these energies was found to be weak, about 0.5% as strong as first order while second order from the mosaic LiF crystal is as much as 16% as strong as first order.

The limiting sensitivity for the system depends on the minimum signal that can be distinguished from background and electronic noise. For a conservative value of $R_p = 5$ the limiting sensitivity was estimating to be one to two orders of magnitude greater than required to record continuum for the conditions reported by Mead *et al.*⁷

VI. ALIGNMENT

Because continuum spectra are featureless and may not have recognizable features of known energy an absolute energy scale was determined and referenced to the spectrograph. This was done using mechanical references established during bench alignment. A mechanical pointer (Fig. 13) mounted on the collimator and referenced to the spectrograph optical axis was aligned to an x-ray illuminated slit using the monitor output to display the MCP image for correct positioning of the observed spectra. The pointer setting defines both the correct target distance and the optical axis of the spectrograph to which all instruments on the re-entrant assembly are coaligned. Once the correct bench alignment is achieved the pointer can be removed. Its settings are repeatable for alignment in the target chamber. An energy scale is defined by the position of calibration lines in the frame grabbed image and is referenced to the MCP through fiducial marks on the fiberoptic. The alignment of the energy scale to one pixel in the frame grabber field requires lateral alignment of the pointer at the target to an accuracy of ± 0.5 mm. This is easily achieved and maintained. Because all alignment settings are referenced to internal mechanical markers, this energy scale is carried with the instrument. The energy points for

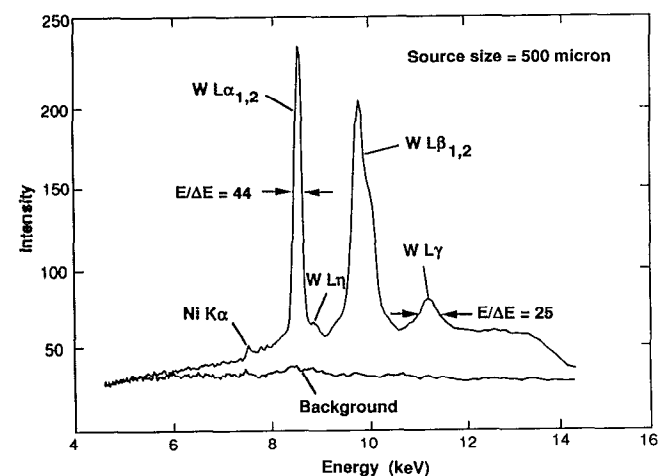


FIG. 15. PET spectrum of tungsten anode showing L -series lines and continuum. Energy resolution is essentially the design resolution for a 500 μm source.

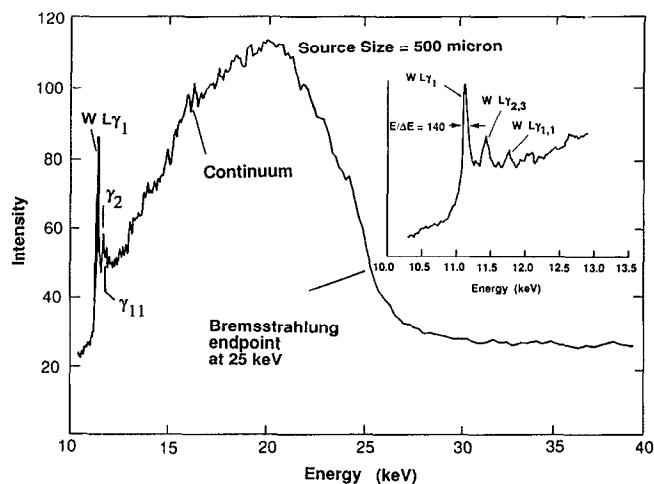


FIG. 16. LiF spectrum of tungsten anode showing $L\gamma$ lines and continuum. Anode was operated at 25 kV to display the bremsstrahlung endpoint. Inset shows details of $W L\gamma$ lines on expanded energy scale. Resolving power is about 140 for the $L\gamma$ lines.

determining the energy scale were obtained from reference spectral lines and from K edge features having well-known energies.

VII. OPERATION

Figure 14 shows a live monitor display obtained with the crystal spectrograph exposed to a 500 μm tungsten x-ray source in a vacuum chamber under conditions meant to simulate conditions in the Aurora target chamber. The beam path from the source window to the detector is evacuated to 10^{-5} Torr and the source is at the laser target position. The integration period for the frame shown here is 0.017 s. Detector sensitivity compared to Kodak DEF x-ray film can be estimated from the fact that an exposure of about 5–10 s is required to show similar detail for these source conditions. This suggests a detector sensitivity at least a hundred times greater than the sensitivity of this

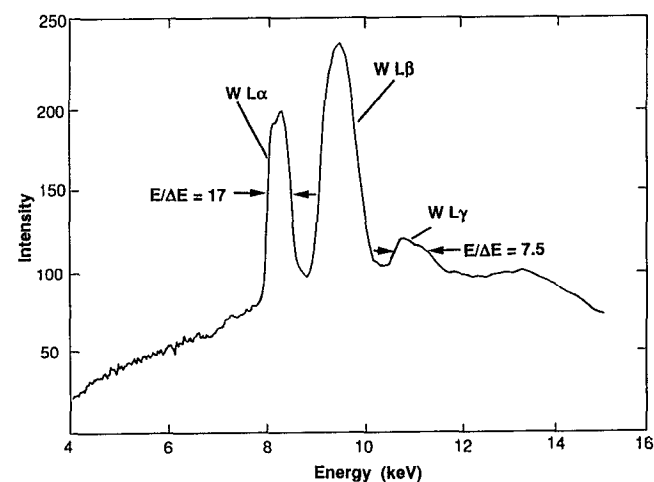


FIG. 17. PET spectrum of extended source. Resolution is consistent with source demagnification expected with convex curved crystal.

film for this energy range. The effectiveness of the shielding can be judged by the very low background.

Figure 15 shows a spectrum taken with the PET channel of the tungsten *L*-series lines. These lines have intrinsic widths corresponding to $E/\Delta E$ of the order of 2000. This greatly exceeds the design resolving power so the observed shape of these lines provides a good measure of the overall instrument function. The measured resolving power for the PET channel is seen to be essentially the same as the design resolving power for a source size of 500 μm . Figure 16 shows spectra taken with the LiF channel for the same conditions. From the width of the W $L\gamma$ lines the resolving power is of the order of 140. No reference lines were available for determining the resolving power at the high energy end of the spectrum where the resolving power is expected to be of the order of 20. The greatest uncertainty here is the spatial resolution of the proximity focused MCP at 35 keV.

To determine the effect of source size on energy resolution spectra were taken of an extended source. Such a spectrum is shown in Fig. 17. The source length in the direction of dispersion is 8000 μm . The resolving power is of the order of 20 at the center of the spectrum and is consistent with the source demagnification expected with a convex curved crystal. This resolving power is compatible with useful continuum analysis for sources that exceed the dimensions anticipated for ICF targets.

ACKNOWLEDGMENTS

We would like to acknowledge the advice and support of Dr. J. Kephart of LANL during the planning and de-

velopment of this instrument. This work was performed under the auspices of U.S. DOE Contract No. DE-AC03-87DP10560.

- ¹D. C. Slater, Gar. E. Busch, G. Charatis, R. R. Johnson, F. J. Mayer, R. J. Schroeder, J. D. Simpson, D. Sullivan, J. A. Tarvin, and C. E. Thomas, *Phys. Rev. Lett.* **46**, 1199 (1981).
- ²R. L. Keck, L. M. Goldman, M. C. Richardson, W. Seka, and K. Tanaka, *Phys. Fluids* **27**, 2762 (1984).
- ³W. Priedhorsky and D. Lier, *Rev. Sci. Instrum.* **53**, 1189 (1982).
- ⁴W. Priedhorsky, D. Lier, R. Day, and D. Gerke, *Phys. Rev. Lett.* **47**, 1661 (1981).
- ⁵H. N. Kornblum, B. L. Pruett, K. G. Tirsell, and V. M. Slivinsky, University of California Lawrence Livermore National Laboratory Report UCRL-81471 (1978).
- ⁶C. L. Wang, *Rev. Sci. Instrum.* **52**, 1317 (1981).
- ⁷W. C. Mead, E. K. Stover, R. L. Kauffman, H. N. Kornblum, and B. F. Lasinski, *Phys. Rev. A* **38**, 5275 (1988).
- ⁸M. de Broglie and F. A. Lindemann, *C. R. Acad. Sci. Paris* **158**, 944 (1914).
- ⁹L. S. Birks, *Rev. Sci. Instrum.* **8**, 1129 (1970).
- ¹⁰A. J. Burek, *Rev. Sci. Instrum.* **61**, 2798 (1990).
- ¹¹B. Yaakobi and A. J. Burek, *IEEE J. Quantum Electron.* **QE-19**, 1841 (1983).
- ¹²A. J. Burek and B. Yaakobi, *Lab. Laser Energetic Rep.* **140** (1983).
- ¹³W. C. Priedhorsky, D. W. Lier, and R. H. Day, *Rev. Sci. Instrum.* **54**, 1605 (1983).
- ¹⁴M. Swartz, S. Kastner, E. Rothe, and W. Neupert, *J. Phys. B* **4**, 1747 (1971).
- ¹⁵M. Gersten and J. E. Rauch, *J. Appl. Phys.* **53**, 1297 (1982).
- ¹⁶J. W. Criss, *Appl. Spectrosc.* **33**, 19 (1979).
- ¹⁷B. Yaakobi and A. J. Burek, *Lab. Laser Energetics Rep.* **137**, (1983).
- ¹⁸J. D. Kilkenny, *Laser Particle Beams* **9**, 49 (1991).
- ¹⁹K. W. Dolan and J. Chang, *SPIE* **106**, 178 (1977).
- ²⁰M. Hirata, N. Yamaguchi, T. Cho, E. Takahashi, T. Kondoh, S. Aoki, H. Maezawa, and A. Yagishita, *Rev. Sci. Instrum.* **61**, 2566 (1990).
- ²¹Reynolds Industries Inc., 5005 McConnell Ave., Los Angeles, CA 90066-6734.